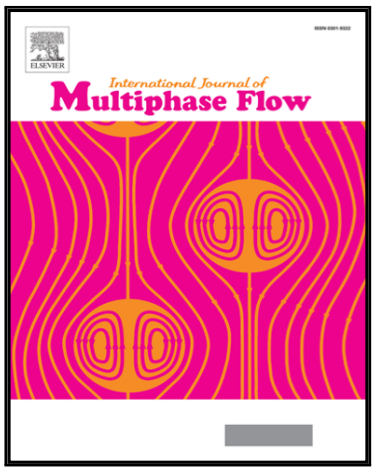

Experimental Study on Steam Chugging Phenomenon in a Vertical Sparger

Giuseppe Gregu , Minoru Takahashi , Marco Pellegrini , Riccardo Mereu

PII: S0301-9322(16)30048-9
DOI: 10.1016/j.ijmultiphaseflow.2016.09.020
Reference: IJMF 2478

To appear in: *International Journal of Multiphase Flow*

Please cite this article as: Giuseppe Gregu , Minoru Takahashi , Marco Pellegrini , Riccardo Mereu , Experimental Study on Steam Chugging Phenomenon in a Vertical Sparger, *International Journal of Multiphase Flow* (2016), doi: 10.1016/j.ijmultiphaseflow.2016.09.020

Highlights:

- Experimental study on the mechanisms of every phase of the Chugging cycle in direct contact condensation
- Pressure pulses measured at two positions inside the pipe and synchronized with images from a high speed video camera
- Low pressure condition inside the bubble might be the cause of interfacial instability which generates the bubble collapse
- High pressure peaks characteristics of Chugging are caused by the condensation induced water hammer phenomena inside the pipe
- Creation of a chugging regime map based on collected data

Experimental Study on Steam Chugging Phenomenon in a Vertical Sparger

Giuseppe Gregu [a], Minoru Takahashi [b], Marco Pellegrini [c], Riccardo Mereu [a,*]

a Politecnico di Milano, Piazza Leonardo da Vinci 32, 20133 Milano, Italy.
b Research Laboratory for Nuclear Reactors, Tokyo Institute of Technology, N1-18, 2-12-1 Okayama, Meguro-ku, Tokyo, 152-8550 Japan.
c The Institute of Applied Energy, Shimbashi SY Building, 1-14-2 Nishi-Shimbashi 1-Chome, Minato-ku, Tokyo, 105-0003, Japan
* Corresponding author, riccardo.mereu@polimi.it, tel: 0039 0223993830

Abstract

Unstable direct contact condensation called "Chugging" that occurs in certain conditions in the pressure suppression pool of Primary Containment Vessel of Boiling Water Reactors (BWRs) was studied experimentally. The mechanisms of every phase of the chugging was described, and experimental results useful for the development and validation of more accurate CFD models were provided. The experiment was conducted with a transparent pool and a transparent polycarbonate pipe or a stainless steel pipe with inner diameter of 27mm under the conditions of the steam mass flux of 5.5 - 19.5 kg/m^{2}s and the pool temperature of 19 - 46.5 °C. Pressure pulses were measured and synchronized with a high speed video camera for images acquisition. It was identified that the bubble implosion occurred while the pressure in the bubble quickly decreased. This condition might establish instability in the interfacial area which grew abruptly causing the implosion. Moreover the transparent apparatus allowed to interpret and relate internal condensations, generating pressure spikes of around 1.2 MPa because of the condensation-induced water hammer. Finally, the chugging condensation regime map was created from the experimental data.

Keywords

Condensation; Direct Contact; Chugging; BWR; Bubble; Pressure Spikes.

1. Introduction

Direct contact condensation is used in the pressure suppression pool in the Primary Containment Vessel of nuclear boiling water reactors (BWRs) to reduce the pressure of steam generated by the flashing of water during a loss of coolant accident [1]. The direct contact condensation is characterized by no solid boundary wall between vapor and subcooled liquid, which results in higher condensation heat transfer than that of usual condensation. The direct contact condensation technique is also used in many industrial applications such as chemical and marine industries [2]. However, an unfavourable instability called "Chugging" occurs under specific conditions given by three parameters - water subcooling, steam mass flux and pipe inner diameter. In order to find the conditions of suppressing the chugging, the direct contact condensation and chugging phenomena have been investigated so far.

Some of the researchers focused on developing two dimensional condensation regime map [1], [3], [4], [5]. Petrovic de With et al. [2] presented a three dimensional condensation regime map, adding the injector size diameter as a fundamental parameter. Table 1 gives a summary of the previous experimental studies [6], [7], [8]. Pressure signals during chugging [9], [10], [11], [12], [13], [14], [15] and the effect of the direct contact condensation on the pool temperature stratification [16], [17] were studied. They described the phenomena through the definition of main parameters without explaining the physical mechanism. Violent internal condensations inside a sparger pipe caused by the condensation induced water hammer was explained by Urban et al. [18] and the associated pressure spikes during chugging regime were detected by Purhonen et al. [12] and Laine et al. [13]. Air or other non-condensable gases addition to the steam flow has been identified as a valid technique to suppress the chugging effects [19, 20, 21]. As reported by Liang & Griffith [19] and Zhao et al. [21] in their study an amount lower than 1% of air in the steam flow can drastically reduce or eliminate the chugging appearance. They found the air content in steam is function of Reynolds, Jacob and Prandtl numbers and fluid properties [19].

Recent studies focused on steam–water interface oscillations induced by pipe blowdown steam injection into a pool with sub-cooled water. The relationship between amplitude and frequency has been analysed using different approaches. The momentum source has been used to relate the amplitude and frequency of oscillations in the pipe to a synthetic jet analogy [22] and to the Richardson number, used then to determine the occurrence of thermal stratification [23]. Villanueva et al. [24] identified the Froude

number as similarity criterion for a scaled non-dimensional amplitude and frequency representation of the system behaviour analysing a set of available experimental data at different scales. They found the scaled amplitude has a maximum at Fr ≈ 2.8 and the scaled frequency a minimum at Fr ≈ 6 observing a strong dependence on temperature from Fr > 6, with higher scaled frequency at lower bulk temperature.

Ueno et al. [25] investigated experimentally the bubble collapse at low steam velocities in order to take into account only the condensation mechanisms, and suggested that that the collapse occurred once small disturbances arise on the bubble surface. Assuming a symmetrical bubble they found out that the bubble reached the maximum volume at first and then it start shrinking because of the enhancement of the condensation caused by the necking of the bubble and the abrupt shut off of steam injection. Only when the volume decreased and the pressure inside the bubble was low, tiny disturbances of O (100μm) arose on the surface and the collapse occurred. Through the evaluation of the bubble radius and its second derivative with respect to time they asserted that the instability on the condensing vapor bubble was not the Rayleigh-Taylor type in their experiments.

Recently, CFD analysis was applied to the chugging phenomenon to validate proposed models. Tanskanen [26, 27, 28, 29, 30] performed a comprehensive CFD study of two-phase flow for the prediction of the direct contact condensation employing two-fluid model. Their work focused on the description of the heat transfer coefficient given by the turbulent flow around the bubble surface as the main parameter characterizing the bubble implosion. Their work produced interesting results but showed limitations in the prediction of chugging and generality of the model.

Pellegrini et al. [31] added an analytical model of interfacial wave growth to the work of Tanskanen based on the Rayleigh-Taylor instability theory, and produced encouraging results for the prediction of chugging. They developed an analytical model representing the increase of the bubble interfacial area based on the Rayleigh-Taylor instability model and applied to CFD validation. They proposed that the reduction in pressure observed triggered the Rayleigh-Taylor instability, because the pool water accelerated toward the lighter steam and waves developed on the interface. This growing waves were responsible for an exponential increasing interfacial area and thus the collapse of the bubble.

In the present study, the mechanisms of every phase composing a chugging cycle are investigated, and experimental results useful for a more accurate interpretation of the phenomena and for the development of suitable models are provided.

Table 1 Experimental studies related to chugging phenomena and bubble collapse

Ref.	Pipe inner diameter [mm]	Pool temperature [°C]	Mass flux [kg/(m^{2}s)]	Vapor properties	Pipe orientation	Measurement and location	Notes
Petrovich de With et al. [2]	10 - 50	10 - 100	0 - 200				Based on the other's experiments.
Aya et al. [3]	18.29	10 - 85	0 - 40	101.3 kPa	Vertical	Pool temperature at 5 cm from pipe outlet	
Chan et al. [4]	50.8	40 - 90	0 - 175		Vertical	Movies, temperature at the pipe outlet, and pressure in pipe and pool	Superheated steam. Steam dump for degassing. Control of the pool temperature.
Cho et al. [5]	5 - 20	20 - 95	24 - 1190	Maximum 103 kPa, x>99%	Horizontal	Static pressure in pool, movies, and temperatures in pool.	Calibration of the flow meter with the constant volume method.
Youn et al. [9]	15.9 and 19	20 - 70	10 - 80	Maximum 980 kPa	Horizontal	Movies taken with high speed camera and synchronous pressure in pool. Temperature far from the outlet	High pressure steam. Loop to control the pool temperature. No effect of pipe material and drywell

Marks et al. [10]	25.4, 4.5, 101.6 and 304.8	20 - 90	10, 20, 30	Saturated condition, 690 kPa	Vertical	Pressure in pipe, and temperatures in pipe and pool. Air flow rate.	No effect of drywell. Installation of a steam dump. Development of an analytical model.
Nariai et al. [11]	18.29	20 - 80	0 - 200		Vertical		Linear frequency analysis.
Purhonen et al [12]	85, 110, 214	11 - 76	4 - 13	300 – 3000 kPa	Vertical	Pressure in pipe, and temperature in pipe and pool. Movies taken with high speed camera.	Detection of high pressure peaks inside the pipe. Low fps of the camera. High pressure steam.
Class et al. [14]		25	20	117 kPa	Vertical	Movies taken with high speed camera. Temperature in pipe and pool. Pressures with strain gauges in pipe.	Steam pressure equals to 117 kPa. Only 4 chugging cycles per experiments.
Liang et al. [19]	19	60 - 90	0 - 50	Slightly above atmospheric	Vertical, upward		Investigation of the effect of air in suppressing chugging.
Araneo et al. [20]	200	10 - 100	1, 3		Vertical	Temperatures in pool. Movies taken with high speed camera.	Investigated the effect of air on chugging. Nearly constant water level during the experiments.
Solom et al. [16]	38	40 - 100	34 (steam + water)	101 – 200 kPa	Vertical	Temperatures in pool with arrays of thermocouples.	Deionized water pool. Hot water from the pool is sent inside the steam generators.
Song et al. [17]	4.2	40 - 88	3.06 - 19		Vertical	High speed camera and halogen lamp system.	Heaters in the steam line to prevent condensation. Experiment under sub-atmospheric pressure.
Ueno et al. [25]	2	30 - 100		101°C	Vertical, upward	Movies taken with high speed camera. Control of pool temperature with a cooling loop. Single bubble generation.	Bubble implosion analysis related to a different field from chugging.
Sargis et al. [15]	22.25	20			Vertical	Pressure in pool and pipe. Movies taken with high speed films	Analytical model compared with experimental results.

2. Experimental apparatus and procedure

2.1 Experimental apparatus

The experimental apparatus is shown in Fig. 1. It is composed of the boiler tank, the steam line, the two evacuation lines and the test section. A detailed explanation of the apparatus can be found in [32].

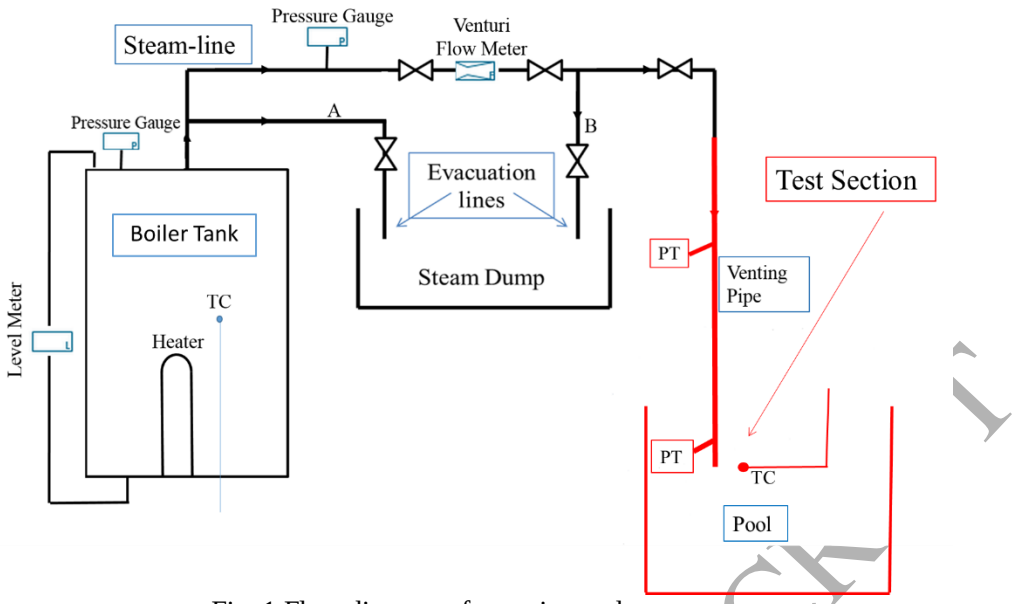

Fig. 1 Flow diagram of experimental apparatus

The water is heated to the boiling point in a 150.7 cm^3 stainless steel cylindrical shape main tank properly insulated. Heaters of 36kW were installed in the boiler tank for the generation of the steam. A K-type sheathed thermocouple (TC) was inserted inside the main tank to measure the water and steam temperature and to detect the moment of insurgence of the boiling. The produced steam was sent to the test section through an insulated steam line and the steam flow was controlled through three operation valves. The measurement of the steam flow rate was obtained with a flow meter consisting of a Venturi tube inserted in the steam line and a differential pressure transducer, Yokogawa DPF110 4-20 mA 1-5V, which evaluates the pressure difference created in the convergent section. The presence of non-condensable gases in the flow could have a large effect on chugging behavior. For this reason the non-condensable gases were removed through the injection of the steam in the steam dump before the experiments.

The test section consisted of the venting pipe and the transparent pool made of acrylic resin. The venting pipes were made of stainless steel and transparent polycarbonate pipes with 27 mm in inner diameter. The polycarbonate pipe which had good mechanical properties at temperature below 120 °C allowed to visualize the behavior of the interface inside the pipe, while the stainless steel pipe assured excellent properties even under high dynamic loads. Two pressure taps were located at 3 cm and 50 cm upstream from the outlet of the venting pipe: the first one allowed a better investigation of the chugging phases in which the interface was close to the outlet, and the second one was suited to analyse what happens when the interface was abundantly inside the pipe.

The pool tank was made of an acrylic resin cube with side lengths and depth of 50 cm that was open at the top side. The water pool temperature was kept lower than the maximum allowable temperature 70 °C, i. e., high subcooling. The pool temperature was not controlled through an external circulation loop, but only monitored as Marks et al. [10] by a K-type sheathed thermocouple placed at the same level of the pipe outlet and 3 cm distant from the pipe axis. Table 2 summarizes the main properties of the test section.

Table 2 Specifications of test section

	Materials	Dimensions	Measurement items
Venting Pipe	Polycarbonate, Stainless steel	27 mm (Inner diameter ϕ)	Static pressure
		75 mm (Submersion depth in water pool)	
Water Pool	Acrylic resin	500x500x500 mm	Water pool temperature

2.2 Measuring instruments and data acquisition system

The arrangement of measuring instruments in the test section are shown in Fig. 2 as a top view. Static pressures at two locations in the venting pipe were measured using semiconductor pressure transducers connected to pressure taps mounted on the pipe wall. The first pressure transducer is a JTEKT Corporation

PMS-5M-2 while the second one is a PMS-m5-SN8006: due to the external pressure, a deformation is induced in a lamina and its electrical resistance change proportionally with it. In order to evaluate the variation of resistance a bridge circuit was built. The pipe has been secured to the upper part of the pool with a rigid support at 10cm from the lower exit. Pressure transducers are positioned into the lateral insertion of the pipe taking care to fill all the connecting parts with water to avoid any kind of delay or signal damping. A high speed camera with both transparent pipes and pool and two synchronous pressure signals inside the pipe were used in order to link the different phases of the phenomenon with quantitative data. A high speed camera (Photron FASTCAM SA5), especially when combined with the installation of a polycarbonate venting pipe, was used to observe chugging phenomena with frame speed of 1000 - 5000 fps. A metal halide lamp was used to illuminate the scene.

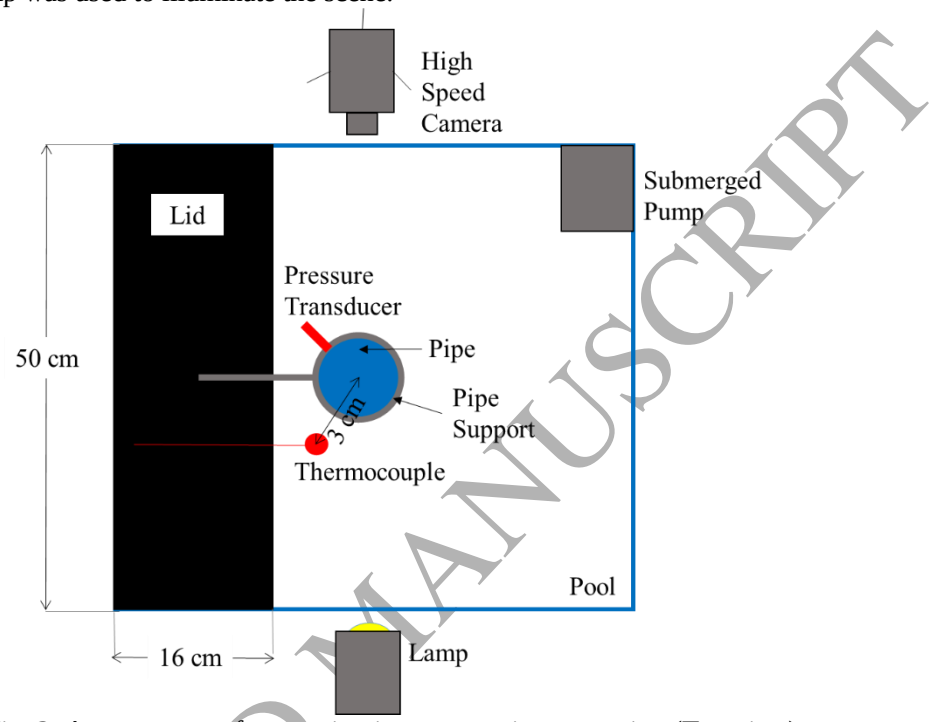

Fig. 2 Arrangement of measuring instruments in test section (Top view)

A schematic drawing of the data transfer is shown in Fig. 3. A TTL signal was generated when the camera trigger started and it constituted the time zero of the experiment allowing to have a perfect synchronization between the images and the pressure transducers signal. The delay of the signals due to the transmission of around 5 ns/m of cable was abundantly shorter than the time scale of phenomena of around 0.1ms. The signals of the pressure and the control signal of a high speed video camera were data-acquired by the system (TEAC es8) with maximum sampling frequency of 5 kHz. The outputs of the flow meter, the thermocouples in the boiler tank and the water pool tank were monitored using the data acquisition system (Cadac 21, Eto Denki 9220A).

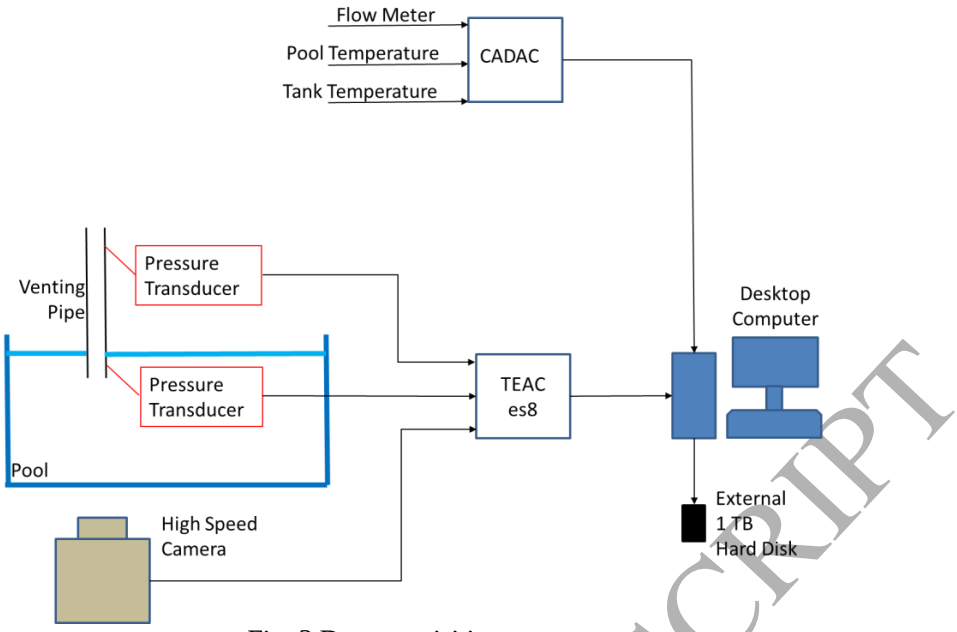

Fig. 3 Data acquisition system

2.3 Experimental procedures

Water in the boiler tank was heated up with the electrical heaters until reaching slightly superheated conditions and the pipe connecting tank and pool has been insulated by using an insulator with 2cm thickness. When the steam started to be produced, it was ejected for 15 minutes outside of the building for removing non condensable air from the flow. As soon as the air was completely removed from the steam flow, the evacuation lines were shut and the pure steam pushed out the residual air from the vertical section of the pipe. This procedure allowed to have only steam coming out from the venting pipe. Two different kinds of experiments were implemented:

In the first type, the signal of the pressure transducers and the video images were recorded simultaneously. This kind of experiment lasted no more than 1 minute. Indeed, in this period of time, because of the high speed of the phenomena, roughly 20 chugging cycles were recorded. The pool temperature rose by less than 1 °C which allowed to consider this quantity as constant. Measurement error of steam flow rate was less than ±0.1 kg/m^{2}s that was negligibly small for the present purpose.

In the second kind of experiment, only pressure signals were recorded without the use of the high speed camera. The duration of the experiment ranging from 15 to 30 minutes was much longer than the former case. Steam flow was kept constant, within the deviation of ±0.1 kg/m^{2}s while pool temperature increased gradually due to the steam ejection inside the pool. The pool temperature in this case was only monitored without being measured.

Experimental conditions are summarized in Table 3. The Froude number is defined as $Fr = G/\left(\rho_s\sqrt{l_s g}\right)$ where G [kg/m^{2}s] represents the steam mass flux, $\rho_s = 0.597518\ kg/m^3$ the steam density, $l_s = 0.075\ m$ the venting pipe submersion depth in water pool, and g [m/s^2] the gravitational acceleration. Froude number values for the present experiments are far from the maximum scaled amplitude and frequency determined by Villanueva et al. [24], as shown in Table 3.

Table 3 Experimental conditions.

Water pool	Pool pressure	Atmospheric
	Pool temperature T_w	19 - 46.5 °C
Steam	Steam pressure (absolute)	Venting pipe exit 0.101325 MPa-a Tank 0.12 MPa-a
	Steam temperature	Venting pipe exit 100°C
	Mass flux G	5.5 - 19.5 kg/m^{2}s

	Froude number Fr	10.73-38
Measurement and observation	Sampling frequency	5000 Hz
	Frame speed of camera	1000 - 5000 fps

3. Experimental Results and Discussion

3.1 Outline of overall condensation behaviors

Instability in interfacial area grew abruptly, which caused the bubble implosion that occurred when the pressure in the bubble quickly decreased. The related internal condensations generated high pressure spikes of around 1.2 MPa due to condensation-induced water hammer, which arose concerns. Based on the data, a chugging condensation regime map was created. The chugging cycle could be divided into five different sequences of events: (i) bubble growth, (ii) bubble collapse, (iii) water suction, (iv) internal condensations, and (v) steam ejection. Fig. 4 (Video 1) shows each phase in a single chugging cycle and its typical time scale of the phenomenon. The sequences of the events are as follows: (1) A chugging cycle began with the bubble formation at the outlet of the pipe. With the increase of the dimension of the bubble, the condensation rate increased and the bubble growth was slowed down until the bubble arrives at its maximum dimension. (2) The bubble suddenly collapsed, which caused a steep reduction of pressure. (3) Water suction occurred inside the pipe. Different small bubble collapses occurred inside the pipe. (4) Internal condensations in the pipe like condensation-induced water hammer occurred. (5) Steam was ejected again.

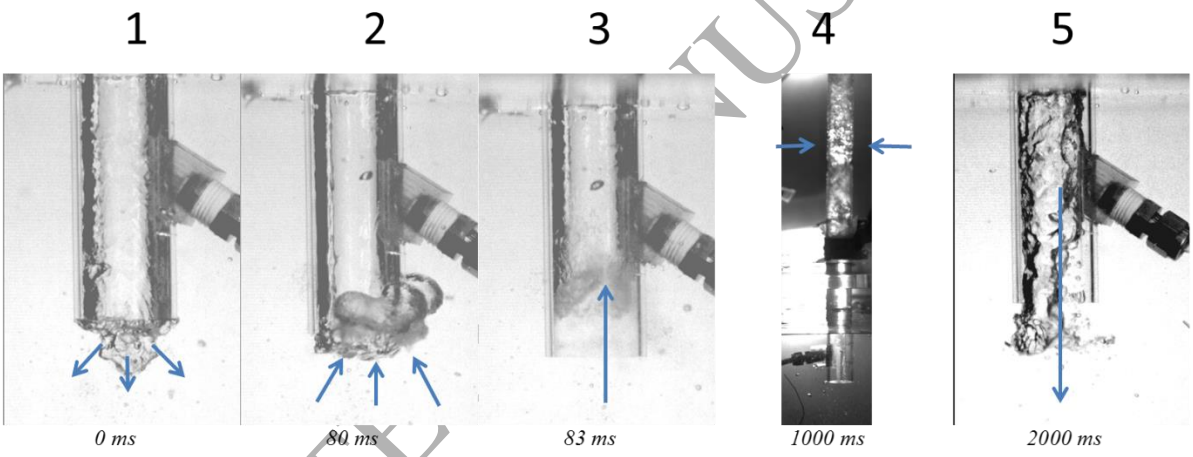

Fig. 4 Characteristic events of chugging cycle

The condensations in the pipe began when the interface velocity became low. It occurred at the time of start of steam flowing down in the pipe or at the time of interface in the pipe reaching the maximum elevation. Condensation behavior in the latter case is shown in Fig. 5 (Video 2).

If the pool water temperature is sufficiently high the formation of a new bubble is observed out of the pipe, otherwise the steam injected in the pool is involved in an abrupt condensation before creating a bubble with sucking water effect into the pipe. Latter case permits the local increase of water temperature until the conditions of a bubble formation outside the pipe.

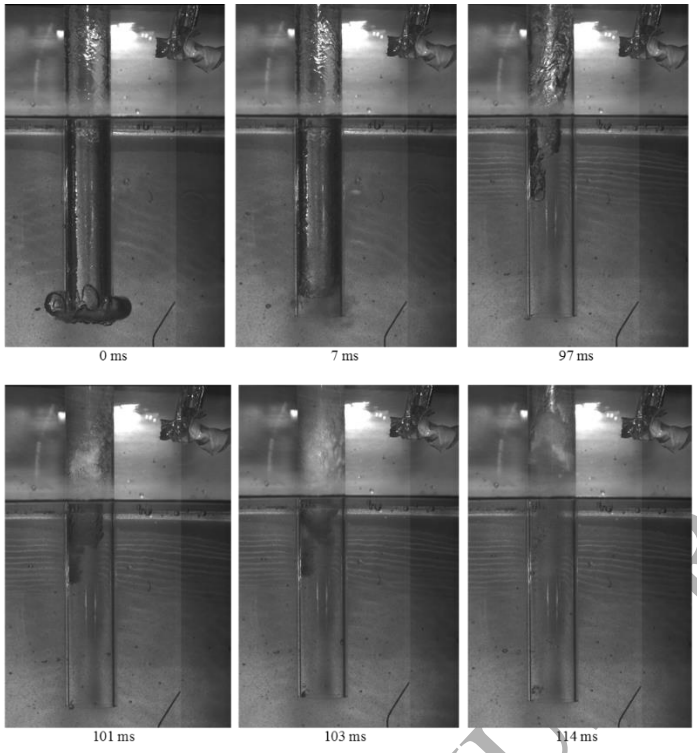

G=5.7 [kg/(m² s)]; Tw=30.3 [°C]; ϕ=0.027 [m]

Fig. 5 Behavior of typical condensation in the pipe

3.2 Behaviors of bubble collapse

Different behaviors of the bubbles are observed, based on steam flow rate and pool temperature. In particular, the bubbles covering and wrapping the pipe vent because of buoyancy force, are defined by Chan & Lee [4] as 'encapsulated bubble'. Fig. 6 shows the behavior of typical collapse of the encapsulated bubble. The encapsulated bubble collapsed suddenly due to an increase of the condensation rate with the modification of the interfacial area. When the bubble is nearly at its maximum size at t =7.167 s, ruffles appeared on the surface, and the heat exchange rate and the condensation rate were enhanced. Initially a small portion of the bubble was involved as seen at t =7.169 s, and the collapse extended to the whole bubble at t =7.170 s.

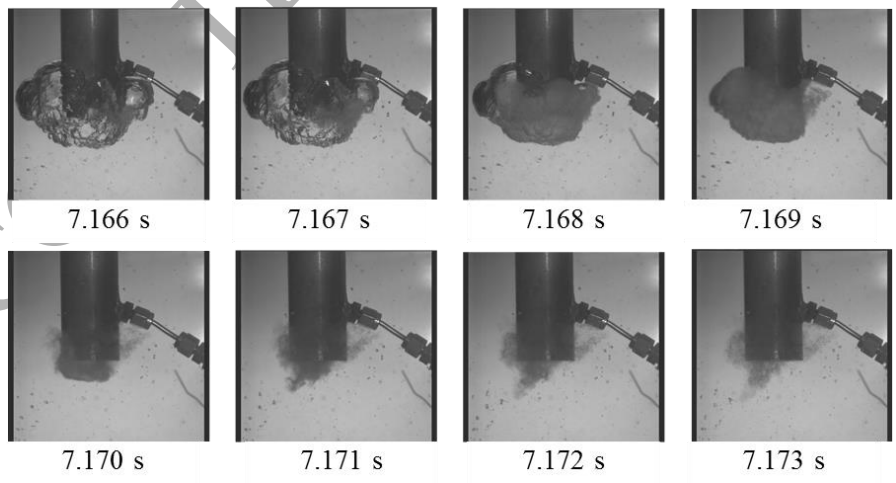

G=15.5 [kg/(m² s)]; Tw=28.7 [°C]; ϕ=0.027 [m]

Fig. 6 Behavior of collapse of an encapsulated bubble

Fig. **6**7 shows the associated measured pressure at locations 3 cm and 50 cm from the outlet of the pipe. During the bubble collapse, the pressure decreased due to the loss of steam mass at 3 cm from the outlet. A decrease of pressure at 50 cm from the outlet was delayed and damped because of the presence of compressible steam in the pipe. This change in pressure caused a suction of water inside the pipe as shown in Fig. 6. Liquid water reached the outlet of the pipe at t = 7.171 s as shown in Fig. 6, which started pressurizing locally the steam so that pressure increases as shown in Fig. 7.

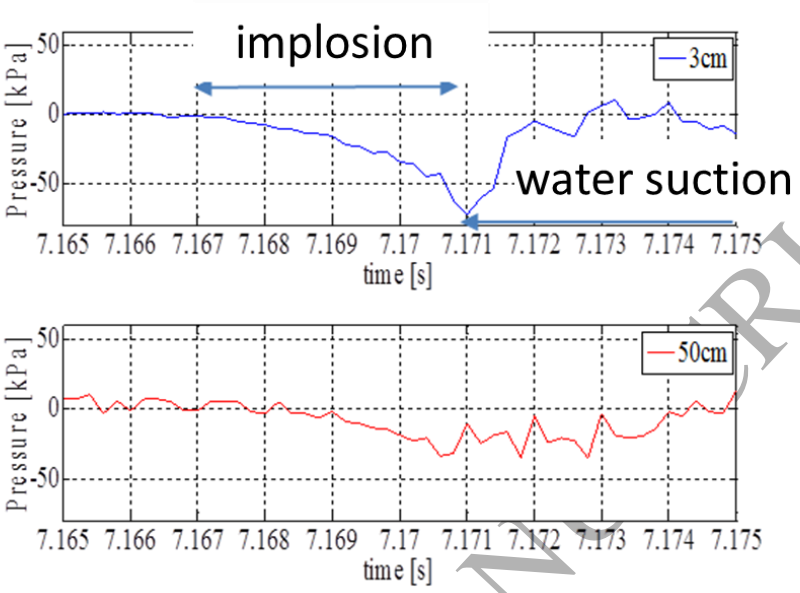

Fig. 7 Static gauge pressure in typical collapse of an encapsulating bubble

Fig. 8 shows the collapse behavior of a non-encapsulating bubble, and Fig. **8** 9 shows the associated pressure at locations 3 cm and 50 cm from the outlet of the pipe. The collapse of non-encapsulating bubbles was faster than for encapsulating bubbles. As measured by the pressure decrease at 3cm from the outlet, the period of time from the start of the bubble collapse until the ending point (at the minimum pressure value) was 2ms for non-encapsulating bubbles vs 3-6ms for encapsulating bubbles.

When the collapse took place, there were a reduction of steam mass and a depressurization around 0.646 s. This caused the suction of water inside the pipe and again pressure increased around 0.648 s because of the acceleration of the liquid towards the surrounding steam.

It is noted that, in chugging phenomena, the necking phase did not take place and thus the supply of steam inside the bubble was continuous on contrary to the theory of Ueno et al. [20]. However the two theories of Ueno et al. [20] and Pellegrini et al. [21] on the onset of instabilities at the time when low pressure appeared inside the bubble were in a good agreement with what observed in the present experiment. The study carried out by Jiguo et al. [33] analyses a condensation regime with presence of Microbubble Emission Boiling (MEB), explaining the interface instability appearance with the presence of microbubbles. A cause-effect relationship between low pressure observed in this experiment and the MEB cannot be clarified with the available information and additional analytical or numerical models are necessary to support this theory.

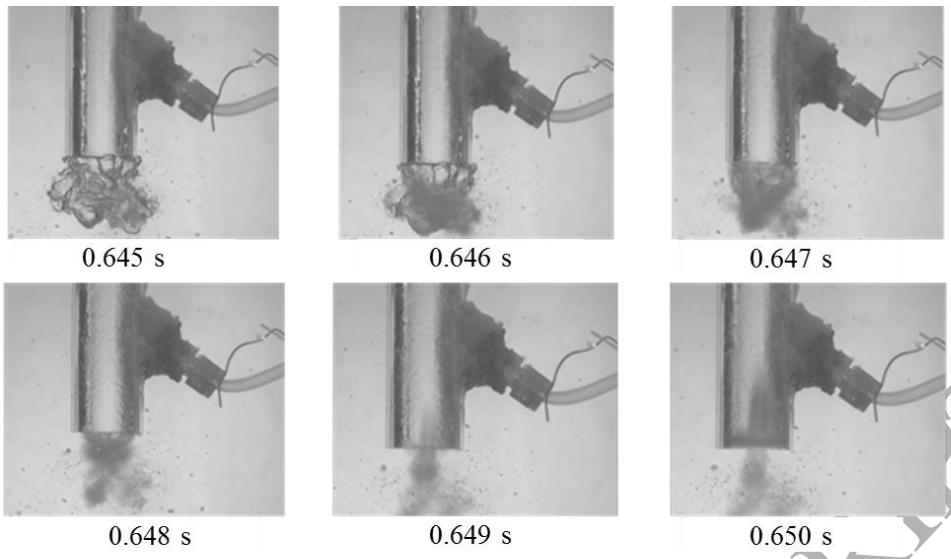

G=9.7 [kg/(m² s)]; Tw=19.5 [°C]; ϕ=0.027 [m]

Fig. 8 Behavior of collapse of a non encapsulating bubble

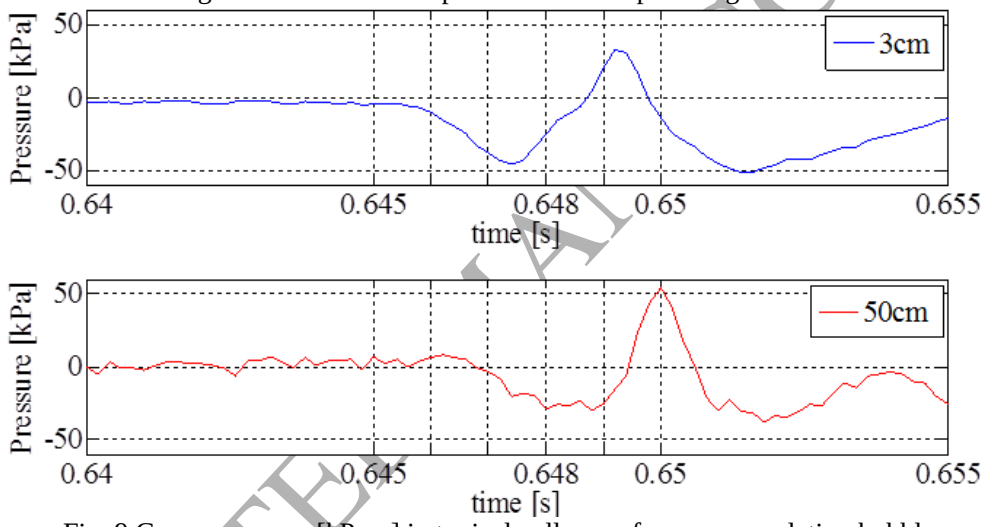

Fig. 9 Gauge pressure [kPa-g] in typical collapse of non encapsulating bubble

3.3 Behavior of internal condensation

High pressure peaks appeared in the internal condensations due to the condensation-induced water hammer caused by the confinement of the pipe and the presence of cold water sucked into the pipe from the bulk of the pool. The intensity of the pressure peaks were higher than the ones of the bubble collapse at the outlet. Fig. 10 shows an example of the pressure peaks. The maximum peak, around 1.2 MPa was in more than an order of magnitude higher than the ones in the bubble implosion phase (around 50 kPa). The three peaks observed in Fig. 10 are related to different violent condensations inside the pipe. Peaks of the gauge pressure lower than -100kPa-g reported in Fig. 10 can be explained by the non-equilibrium condition occurring during the sudden condensation, with a related local sub-atmospheric condition inside the pipe. During this phenomenon the sensor surface of the pressure transducer is pulled by incompressible liquid motion, due to the bubble collapse in a very short time without instantaneous vaporization of the liquid, having as a result the negative sensor signal. In this case three consecutive condensation induced water hammers occurred. An example of the difference between bubble implosion and water hammer

signal can be observed in the synchronized video with pressure signal reported in

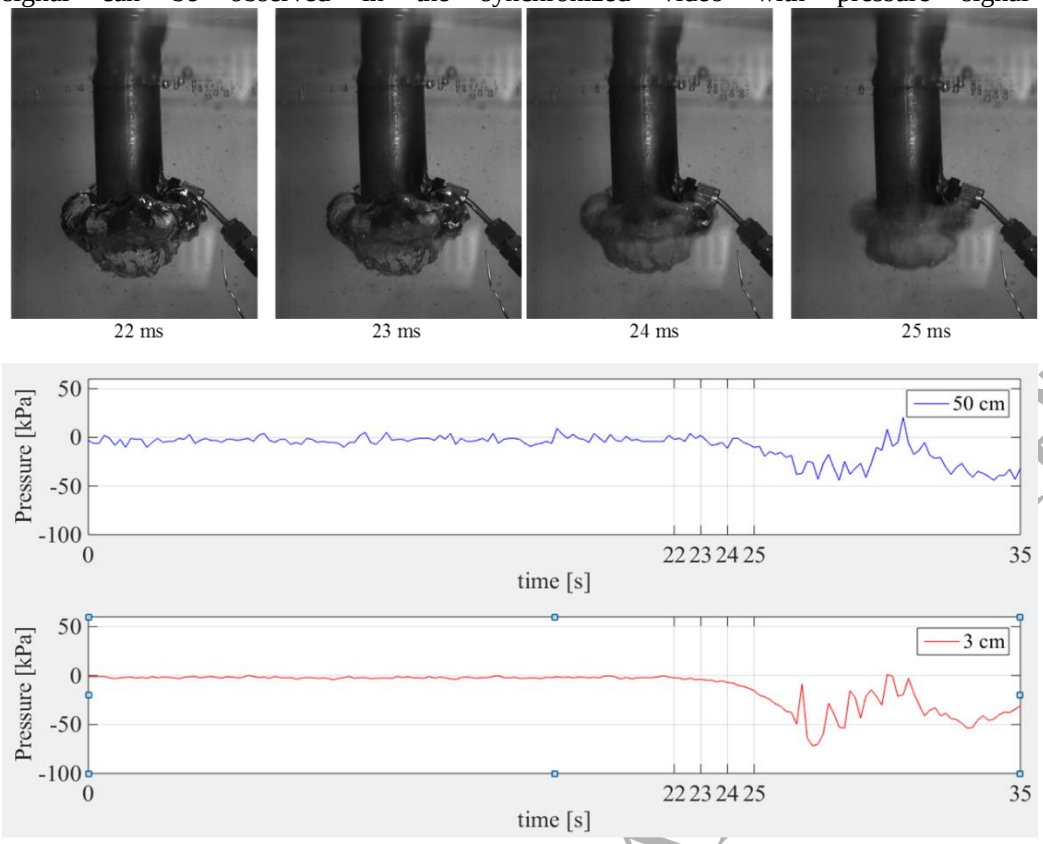

G=15.4 [kg/(m2s)]; Tw=33.8 [°C]; ϕ=0.027 [m]

Fig. **12** (video 3).

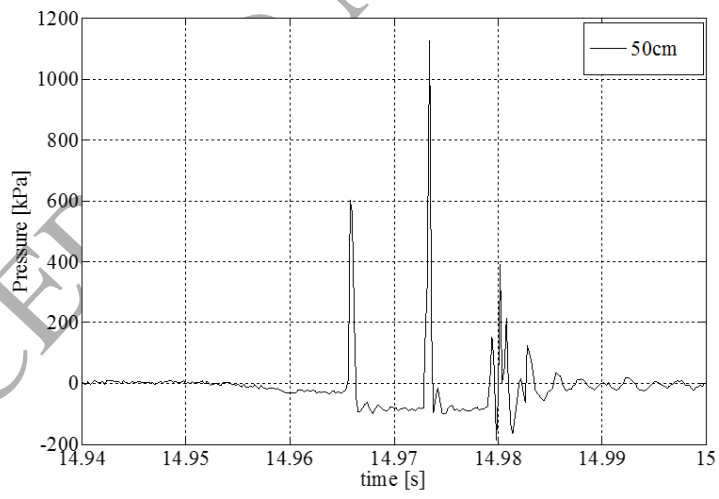

G=6.7 [kg/(m^2 s)]; Tw=24.3 [°C]; ϕ=0.027 [m]

Fig. 10 High gauge pressure [kPa-g] peak at 50cm from outlet due to internal condensation

A series of long experiments at constant flow rate were performed to measure the pressure peaks due to the small bubble implosion inside the pipe. The monitored pool temperature increased gradually because of heating by the continuous ejection of the steam. Fig. 11 shows the results of the number of pressure peaks per unit time in the long experiments with the parameters of the pool temperature and the steam mass flux.

It is found that high frequency of the pressure peaks occurred at low pool temperature and low steam mass flux. Low pool temperature can easily cause the collapse when the water rises inside the pipe and

encounters isolated steam bubbles. On the other hand, if the steam mass flux is low, the interface stayed inside the pipe for longer time because it took longer to decrease the condensation rate and to eject again steam out of the pipe. The two conditions for high frequency of the pressure peaks were coincident with the one relative to the creation of small encapsulating bubbles, which meant that damages because of the pressure peaks were more possible when this kind of bubbles was observed at the outlet of the pipe.

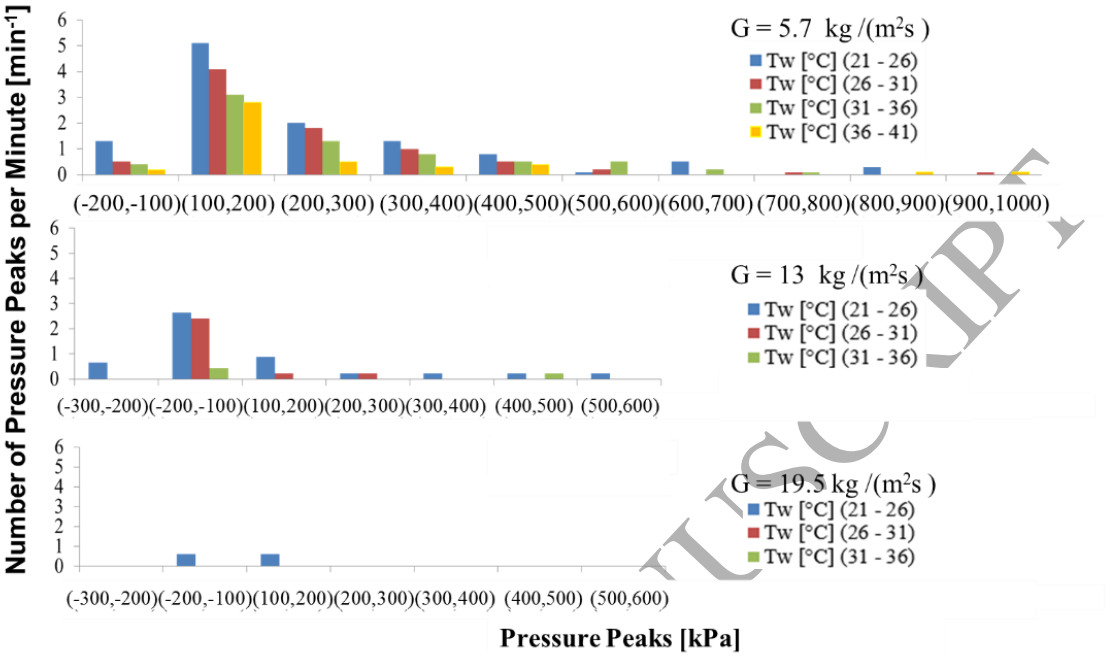

Fig. 11 Effect of mass flux and pool temperature on frequency of occurrence of gauge pressure [kPa-g] peaks

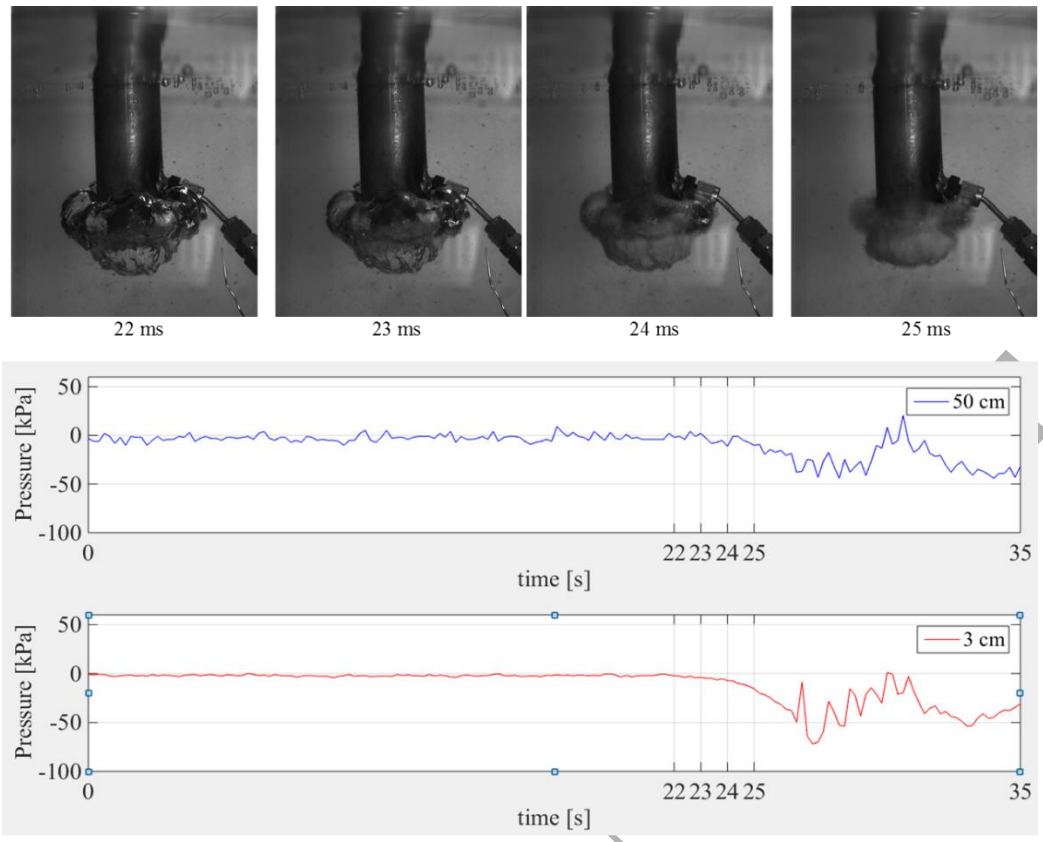

G=15.4 [kg/(m2s)]; Tw=33.8 [°C]; ϕ=0.027 [m]

Fig. 12 Synchronized video with gauge pressure signal [kPa-g]

3.4 Bubble shapes

Fig. 13 shows the chugging regime map ad-hoc built to see the effects of the steam mass flux and the pool temperature on chugging mechanism. Every number in the map represent the experiment label and their detail are given in appendix. Different regions on the map were identified cataloguing the bubbles depending on their shape and on the encapsulation around the pipe [4]. The map is mainly divided by a red thick solid curve into two parts: small chugging and internal chugging, using the terminology from Nariai et al [11]. The internal chugging area is divided by blue thin lines into the following four regions: (i) Small Encapsulating Bubbles, (ii) Big Encapsulating Bubbles, (iii) Big Encapsulating Elongated Bubbles, and (iv) Non encapsulating Bubbles. The small encapsulating bubbles occupy the region of low water temperature and low steam mass flux, where the condensation rate was high due to the cold water but, on the other hand, the inlet steam inside the bubble was small. This caused the formation of small bubbles that encapsulated the pipe because of the dominance of the buoyancy force due to the inertia of the steam.

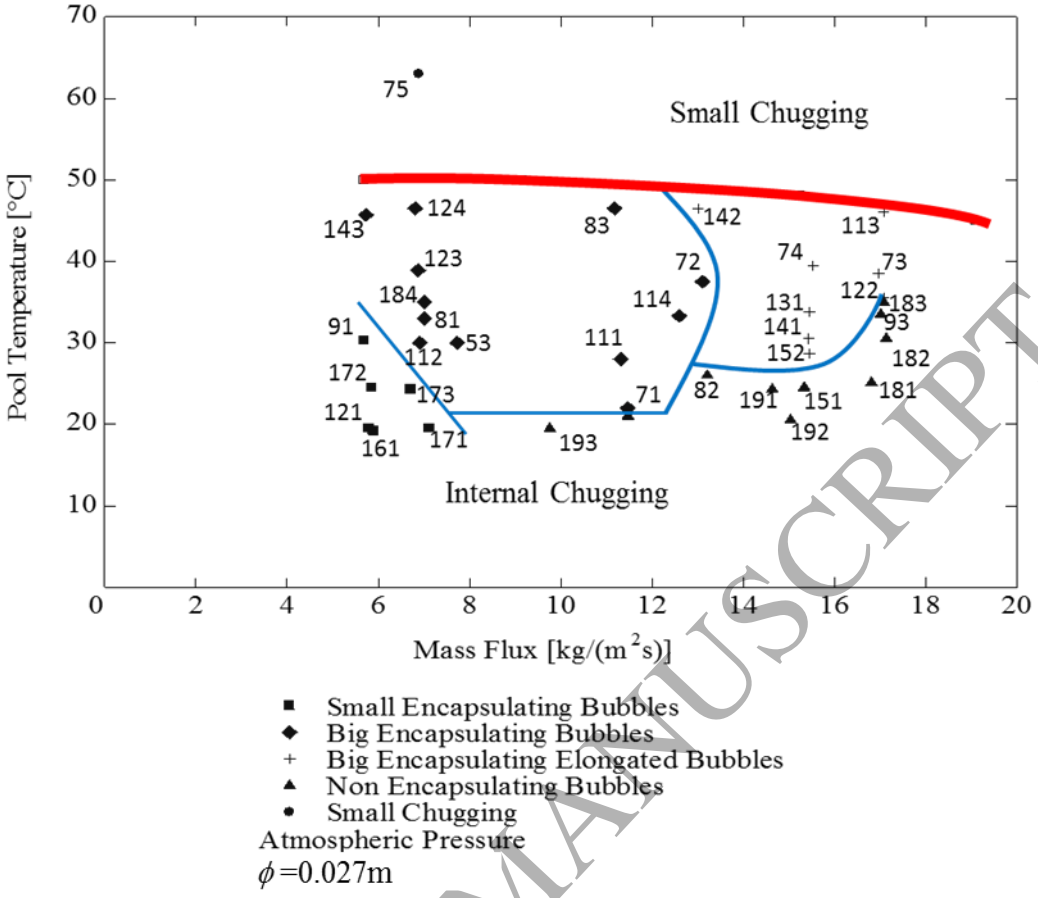

Fig. 13 Chugging regime map

Fig. 14 shows six small encapsulating bubbles representative of the six experiments conducted in this region. The number at the bottom of every picture represents the experiment label. Fig. 15 shows the big encapsulating bubbles characteristic of every experiments and the correspondent experiment label. The area of the big encapsulating bubbles covers most of the map. The dimensions were considerably bigger than the bubble analysed before, especially considering the level of encapsulation of the bubble around the pipe. Fig. 16 shows the big encapsulating elongated bubbles. In this region the inertia of the steam can contrast the buoyancy so that the bubbles assume an elongated form. Fig. 17 shows the examples of non-encapsulating bubbles where the bubbles did not encapsulate the pipe due to the inertia and due to the high condensation rate because of the low water temperature. The creation of these unstable bubbles can be explained with a very fast phenomenon: steam had no time to gradually heat up the surrounding water and form the bubble. Both the growing and the collapse appeared to be significantly faster than the rest of the map.

When the transparent polycarbonate pipe was used, it was possible to note the annular flow of droplets entering the bubble from the pipe during the growth for every bubble shape in Fig. 14 through Fig. 17. This appear as a black layer next to the pipe wall.

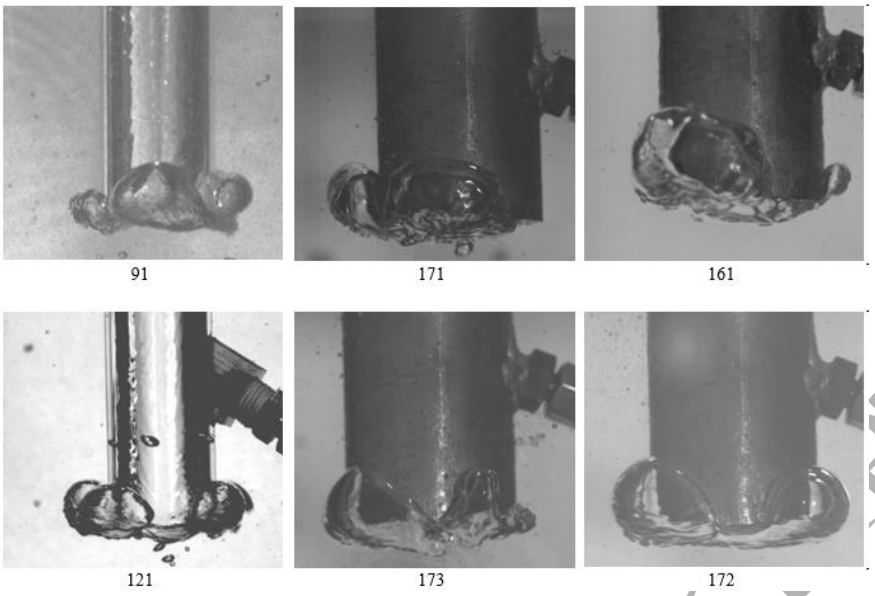

Fig. 14 Behavior of small encapsulating bubbles.

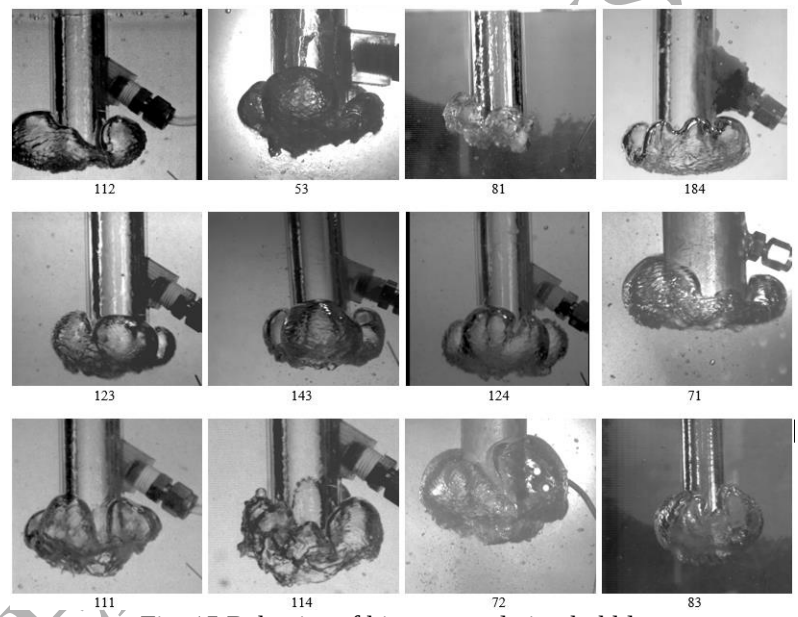

Fig. 15 Behavior of big encapsulating bubbles.

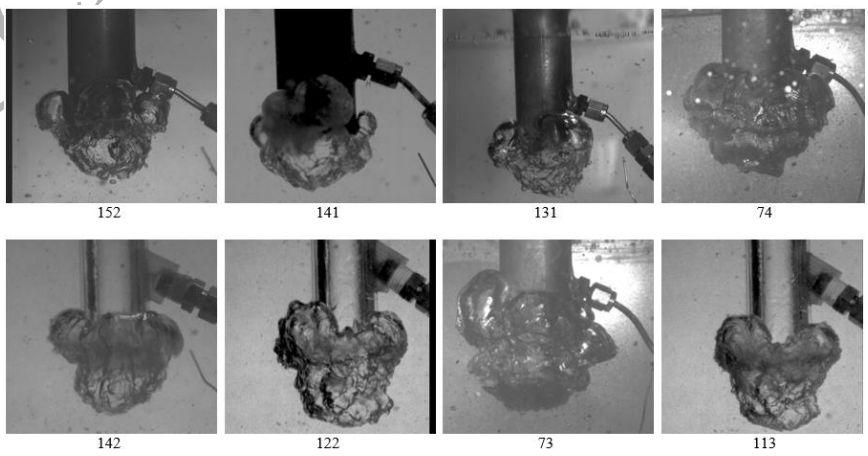

Fig. 16 Behavior of big encapsulating elongated bubbles.

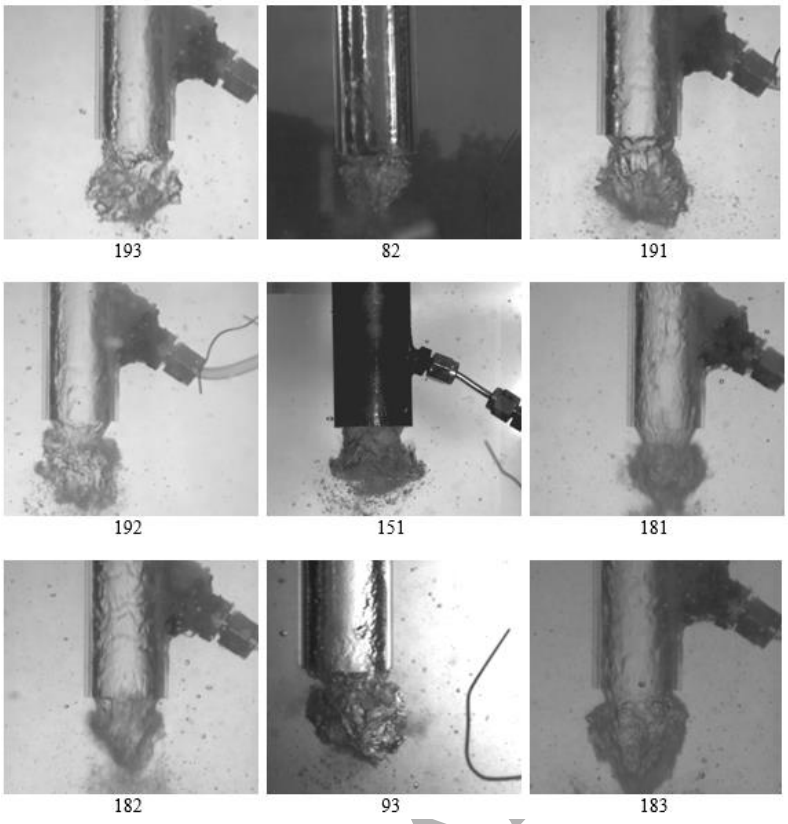

Fig. 17 Behavior of non-encapsulating bubbles.

4. Conclusions

Chugging regime was studied experimentally to investigate the mechanisms of every phase composing a chugging cycle and to provide experimental results for the development and validation of CFD models. Bubble collapse phase was analysed visualizing the images of the high speed camera for both encapsulating and non encapsulating bubbles in relation with the pressure measured at two locations in the steam pipe.

The collapse occurred when the bubble reached its maximum size and pressure suddenly decreased. High pressure peaks characteristics of chugging phenomena were measured with the pressure transducer located 50 cm from the pipe outlet. These pressure spikes were not caused by the bubble implosion whose peaks were always lower than 100 kPa but by the internal condensations inside the pipe. The repetition of these pressure spikes was maximum 10 peaks per minute with an amplitude higher than 100 kPa. The highest pressure peak was 1.2 MPa and the conditions of occurrence were the pool temperature lower than 25 °C and the mass flux lower than 7 kg/m^{2}s. These conditions were highlighted to be the ones characteristic of small encapsulating bubbles formation. This means that every time this type of bubble was observed at the pipe outlet, high frequency of pressure peaks must be expected. This allows to have a simple method for validating analytical and numerical models.

Finally, a regime map was created from the images of a high speed video camera in order to inspect the range of validity of the experimental results. Four different regions were identified in the internal chugging area: small encapsulating bubbles, big encapsulating bubbles, big encapsulating elongated bubbles, and non encapsulating bubbles.

Appendix

Table 4 Experimental results summary.

Experiment name	Mass Flux [kg/(m2s)]	Pool Temperature [°C]	Bubble Shape	Pipe Material
161	5.9	19.2	Small Encapsulating	SS
121	5.8	19.5	Small Encapsulating	P
172	5.9	24.5	Small Encapsulating	SS
91	5.7	30.3	Small Encapsulating	P
171	7.1	19.5	Small Encapsulating	SS
173	6.7	24.3	Small Encapsulating	SS
112	6.9	30	Big Encapsulating	P
53	7.7	30	Big Encapsulating	P
81	7.0	33	Big Encapsulating	P
184	7.0	35	Big Encapsulating	P
123	6.9	38.9	Big Encapsulating	P
143	5.7	45.7	Big Encapsulating	P
124	6.8	46.5	Big Encapsulating	P
71	13.1	22	Big Encapsulating	SS
111	11.3	28	Big Encapsulating	P
114	12.6	33.3	Big Encapsulating	P
72	13.1	37.5	Big Encapsulating	SS
83	11.2	46.5	Big Encapsulating	P
152	15.4	28.7	Big Encapsulating	SS
141	15.4	30.5	Big Encapsulating	SS
131	15.4	33.8	Big Encapsulating	SS
74	15.5	39.5	Big Encapsulating	SS
142	13	46.5	Big Encapsulating	P
122	17.1	35.5	Big Encapsulating	P
73	17	38.5	Big Encapsulating	SS
113	17.1	46	Big Encapsulating	P
193	9.7	19.5	Non Encapsulating	P
82	13.2	26	Non Encapsulating	P
191	14.6	24.3	Non Encapsulating	P
192	15	20.5	Non Encapsulating	P
151	15.3	24.5	Non Encapsulating	SS
181	16.8	25.1	Non Encapsulating	P
182	17.1	30.5	Non Encapsulating	P
93	17	33.5	Non Encapsulating	P
183	17.1	35	Non Encapsulating	P

P = polycarbonate; SS = stainless steel; fps= frame per second.

References

[1] R. T. Lahey and F. J. Moody, The Thermal-hydaulics of a Boiling Water Nuclear Reactor, Second Edition, La Grange Park, Illinois USA: American Nuclear Society.

[2] A. Petrovic de With, R. K. Calay and G. de With, "Three-dimensional condensation regime diagram for direct contact condensation of steam injected into water," *International Journal of Heat and Mass Transfer*, vol. 50, pp. 1762-1770, 2007.

[3] I. Aya and H. Nariai, "Boundaries between regimes of pressure oscillation induced by steam condensation in pressure suppression containment," *Nuclear Engineering and Design*, vol. 99, pp. 31-40, 1987.

[4] C. K. Chan and C. K. Lee, "A regime map for direct contact condensation," *International Journal of Multiphase Flow*, vol. 8, no. 1, pp. 11-20, 1982.

[5] S. Cho, C. H. Song, C. K. Prak and S. K. Yang, "Experimental Study on Dynamic Pressure Pulse in Direct Contact Condensation of Steam Jets Discharging into Subcooled Water," in *NTHAS 98: First Korean-Japan Symposium on Nuclear Thermal Hydraulics and Safety*, Pusan, Korea, October, 21-24, 1998.

[6] IAEA-TECDOC-1677, "Natural Circulation Phenomena and Modelling for Advanced Water Cooled Reactors," Vienna 2012. [Online]. Available: http://www-pub.iaea.org/MTCD/Publications/PDF/TE-1677_web.pdf.

[7] C. H. Song, S. Cho and H. S. Kang, "Steam jet condensation in a pool: from fundamental understanding to engineering scale analysis," *Journal of Heat Transfer*, vol. 134, March 2012.

[8] T. L. Norman, S. T. Rankar, M. Ishii and J. M. Kelly, "Steam-air mixture condensation in a sucooled water pool - final report," Purdue University, West Lafayette, US, December 2006.

[9] D. H. Youn, K. B. Ko, Y. Y. Lee and M. H. Kim, "The Direct Contact Condensation of Steam in a Pool at Low Mass Flux," *Journal of Nuclear Science and Technoloy*, vol. 40, no. 10, pp. 881-885, 2003.

[10] J. S. Marks and G. B. Andeen, "Chugging And Condensation Oscillation," in *18 h National Heat Transfer Conference*, San Diego, California, 1979.

[11] H. Nariai and I. Aya, "Fluid and pressure oscillations occuring at direct contact condensation of steam flow with cold water," *Nuclear Engineering and Design*, vol. 95, pp. 35-45, 1986.

[12] H. Purhonen, M. Puustinen, J. Laine, A. Rasanen, R. Kyrki-Rajamaki and J. Vihavainen, "Steam Blowdown Experiments with the Condensation Pool Test Rig," in *Nuclear Energy for New Europe 2005*,

Bled, Slovenia, Spetember 5-8, 2005.

[13] J. Laine and M. Puustinen, "Condensation Pool Experiment with Steam Using DN200 Blowdown Pipe," Lappeenranta University of Technology, Finland, August 2005.

[14] G. Class, S. Raff and R. Meyder, "The mechanism of violent condensation shocks," *International Journal of Multiphase FLow,* vol. 13, no. 1, pp. 33-46, 1987.

[15] D. A. Sargis, J. H. Stuhmiller and S. S. Wang, "A fundamental thermalhydraulic model to predict steam chugging phenomena," in *ASME 1978 Winter Meeting. Topics in Two-Phase Heat Transfer and Flow*, Del Mar, California, 1978.

[16] M. Solom and K. Vierow, "Experimental Investigation of BWR Suppression Pool Stratification during RCIC System Operation," in *Japan-US seminar on two phase flow*, Purdue University, May 10-15, 2015.

[17] D. Song, N. Erkan, B. Jo and K. Okamoto, "Dimensional analysis of thermal stratification in a suppression pool," *International Journal of Multiphase Flow,* vol. 66, pp. 92-100, 2014.

[18] C. Urban and M. Schluter, "Investigations on the stochastic nature of condensation induced water hammer," *International Journal of Multiphase Flow,* vol. 67, pp. 1-9, 2014.

[19] K. S. Liang and P. Griffith, "Experimental and analytical study of direct contact condensation of steam in water," *Nuclear Engineering and Design,* vol. 147, pp. 425-435, 1994.

[20] L. Araneo, H. Ninokata, M. Ricotti, M. Pellegrini and M. Naitoh, "Suppression pool testing at SIET labs (2) - Steam chugging investigation under the presence of non-condensable gas in a vertical opened pipe," in *10th International Topical Meeting on Nuclear Thermal-Hydraulics, Operation and Safety (NUTHOS-10)*, Okinawa, Japan , December 14-18, 2014.

[21] Q. Zhao, "Effect of non-condensation gas on pressure oscillation of submerged steam jet condensation," *Nuclear Engineering and Design,* vol. 305, no. -, pp. 110-120, 2016.

[22] H. Li, W. Villanueva and P. Kudinov, "Approach and Development of Effective Models for Simulation of Thermal Stratification and Mixing Induced by Steam Injection into a Large Pool of Water," *Science and Technology of Nuclear Installations,* vol. 2014, p. 11, 2014.

[23] D. Song, N. Erkan, B. Jo and K. Okamoto, "Non-dimensional analysis of Thermal Stratification in a Suppression Pool," *International Journal of Multiphase Flow,* vol. 66, pp. 92-100, 2014.

[24] W. Villanueva, H. Li, M. Puustinen and P. Kudinov, "Generalization of experimental data on amplitude

and frequency of oscillations induced by steam injection into a subcooled pool," *Nuclear Engineering and Design*, vol. 295, pp. 155-161, 2015.

[25] I. Ueno, J. Ando, Y. Koiwa, T. Saiki and T. Kaneko, "Interfacial instability of a condensing vapor bubble in a subcooled liquid," *The European Physical Journal*, vol. 224, pp. 415-424, 2015.

[26] V. Tanskanen, *CFD modelling of direct contact condensation in suppression pools by applying condensation models of separated flow*, Ph. D. Thesis, Lappeenranta University of Technology, 2012.

[27] V. Tanskanen, A. Jordan, M. Puustinen and R. Kyrki-Rajamaki, "CFD simulation and pattern recognition analysis of the chugging condensation regime," *Annals of Nuclear Energy*, vol. 66, pp. 133-143, 2014.

[28] J. Laine and M. Puustinen, "Steam Blowdown Experiments on Chugging, Research Report POOLEX 2/2005," Lappeenranta University of Technology, 2006.

[29] S. Banerjee, D. Lakehal and M. Fulgosi, "Surface Divergence Models for scalar exchange between Turbulent Stream," *International Journal of Multiphase Flow*, vol. 30, pp. 963-977, 2004.

[30] E. D. Hughes and R. B. Duffey, "Direct contact condensation and momentum transfer in turbulent separated flows," *International Journal of Multiphase Flow*, vol. 17, no. 5, pp. 599-619, 1991.

[31] M. Pellegrini, M. Naitoh, C. Josey and E. Baglietto, "Modeling of Rayleigh-Taylor Instability for Steam Direct Contact Condensation," in *Proceedings of the 16th International Topical Meeting on Nuclear Reactor Thermalhydraulics (NURETH-16)*, Chicago, USA, August 30 - September 4, 2015.

[32] G. Gregu, "Experimental Study of Steam Chugging Phenomena in Direct Contact Condensation, Master Thesis," Politecnico di Milano, Milan, July 2015.

[33] T. Jiguo, Y. Changqi and S. Licheng, "A study visualizing the collapse of vapor bubbles in a subcooled pool," *International Journal of Heat and Mass Transfer*, vol. 88, pp. 597-608, 2015.

List of figures

List of tables